SMART SENSING SYSTEM FOR ENHANCING THE RELIABILITY OF POWER ELECTRONIC DEVICES USED IN WIND TURBINES

S. H. Teay[1], C. Batunlu[2] and A. Albarbar[1,3]

[1]School of Engineering, Manchester Met University, Manchester, United Kingdom

[3]Correspondent Author: a.albarbar@mmu.ac.uk; Tel.: +44 161 274 6297.

[2] *Department of Electrical and Electronics Engineering, Middle East Technical University, Northern Cyprus Campus, Guzelyurt, Mersin 10, Turkey*

Submitted: Feb. 2, 2017 ***Accepted: Apr. 19, 2017*** ***Published: June 1, 2017***

Abstract: Reliability of modern power systems, in particular those use wind and solar energies, is affected by the relatively short lifetime of the associated power electronic converters (PECs). Thermal stress has been identified as one of the commonest causes for failures in PECs. However, existing thermal monitoring systems are expensive, bulky and with no intelligent capabilities, which limit their full acceptance as monitoring and control tools in operational power plants. This work presents autonomous and inexpensive microcontroller-based system for monitoring and predicting thermal behaviour of switching devices used in PECs. System's inputs are non-intrusively measured voltages and currents drawn by those devices while in operation. The developed system also determines lifetime consumption and has the ability to communicate with external monitoring and control systems e.g. supervisory, control and data acquisition (SCADA) platforms. The performance of the developed system was critically assessed and compared with high-resolution thermal imaging camera. Good agreement between both systems was achieved and the inexpensive developed system was found to have an accuracy of 95%.

Index terms*: Autonomous sensor; lifetime consumption analysis; online rainflow algorithm; dSPACE, finite element, IGBT temperature.*

I. INTRODUCTION

Global warming and recent emission legislations have necessitated more restrictions on the use of conventional fossil power plants. Therefore, renewable energy systems have become the centre of attention as they offer low-cost and environmental friendly source of energy.

The use of wind and solar as clean sources of energy has gained more popularity in the last decade. As a distinctive example Demark generates 25% of its electrical energy from wind, European Union (EU) committed 20% of electricity consumed will be produced by wind energy by 2020 (Natsheh et al. 2012). Power electronic converters (PECs) play a significant role in conditioning and maximising the amount of energy harvested from renewable energy sources, in particular, wind turbine and photovoltaic energy systems (Natsheh et al. 2013).

a. Power electronics in wind turbines

Wind energy systems comprises a rotor with two or three blades that converts wind energy into mechanical rotation energy, a gearbox to increase the rotation speed to that suit the electrical generator attached to it and an electrical generator that converts mechanical into electrical energy. In such system, it is necessary to use power electronic converters (PECs) such as AC-DC rectifiers and DC-AC inverters to enable interfacing to grid and/or functionality of the generator. Two commonly used wind turbine energy systems are shown in in Figure 1.

In general, the generator side rectifier is controlled through a proportional-integrator controller (PI) to obtain maximum electrical torque with minimum current. The maximum rotor power is obtained by using a maximum power point tracking (MPPT) scheme, which controls the optimum rotor speed for each wind speed. On the other hand, the grid side inverter controls the DC-link voltage via the PI controller and ensures the line current to be sinusoidal through a hysteresis controller [2], [6]. Some of the key switching elements used in the converters include Silicon-Controlled Rectifiers (SCR), Gate Turn Off Thyristors (GTOs), Metal Oxide Semiconductor Field Effect Transistor (MOSFET) and Transistors. The Insulated Gate Bipolar Transistor, IGBT, is one of these semiconductor devices which are operated as switching elements in PECs in high switching frequency and current-voltage rating applications (Batunlu et al. 2015). PECs

in renewable energy systems consist of a set of combination of devices such as driver, cooling system, capacitors and power module.

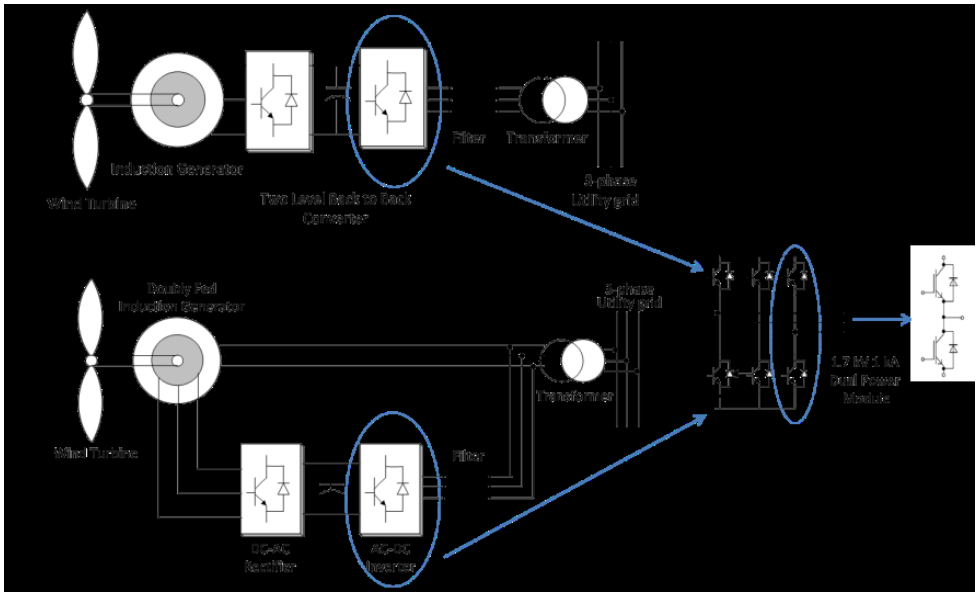

Figure 1. Common wind turbine energy systems (a) induction generator, (b) doubly fed induction generator

Both AC-DC generator side rectifier and DC-AC grid side are serially connected with two IGBT-diode pair and used as one leg of the converter topology as depicted. PECs allow bi-directional power flow between grid and generator side depending on the topology and the application. The wind energy is converted to variable AC voltage/current by generators, therefore the AC-DC and DC-AC power conversion are used to regulate the power. Two and Three Level converters are two most popular types in wind energy applications. Output voltages are smoother with a three-level converter which leads to smaller harmonics but it requires more components and complex control schemes. Two level converters are still preferred in most of the wind applications because of its simpler structure. In general, the generator side rectifier is controlled through a controller to obtain maximum electrical torque with minimum current. The grid side inverter controls the DC-link voltage via another controller and ensures the line current to be sinusoidal through a hysteresis controller.

b. Power electronics in solar photovoltaic systems

   Photovoltaic solar energy systems comprise PV panels that convert solar energy into electrical direct current power (Natsheh et al. 2012). Subsequently, DC-DC

converters are used to step down (or up) that voltage to suit battery charging or inverting into alternating current (AC) and interface to the grid. A block diagram of photovoltaic solar system is shown in Figure 2.

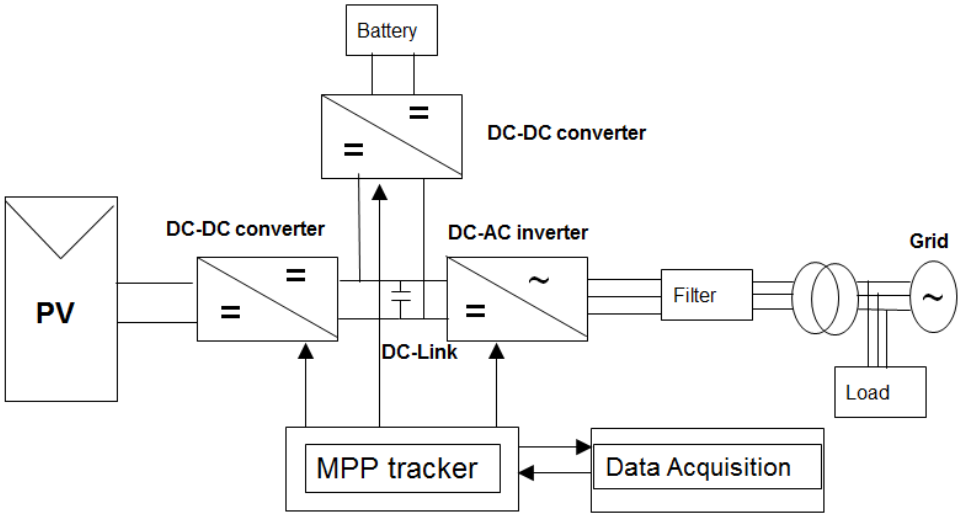

Figure 2. PV system connection to grid and load via DC-DC and DC-AC conversion

c. Energy system common failure modes and causes

As shown in Figure 3a, about 40% of failures in PV solar systems caused by power electronic devices and thus rigorous analysis on the causes of failures in PECs and their lifetime is timely needed (Natsheh et al. 2014). A survey on wind turbine system failures was carried out by (Arabian-Hoseynabadi at.al. 2010) is shown in Figure 3.b arrived at similar conclusions. Most of failures in power electronic converters come from their switching devices due to thermal stresses caused by switching ON and OFF high currents. Insulated gate bipolar transistors (IGBT) are used, typically, as the switching element in PECs due to its large current, high efficiency and fast switching speed. However, electro-thermal stress caused by temperature cycling during switching and conducting phases can ultimately lead to IGBT failures. In order to minimise the probability of sudden IGBT failure, precise real-time monitoring of junction's temperature is crucial to evaluating the overall operational life and hence, reliability of PECs. Some of previous research, which looked into obtaining applicable electro-thermal models for IGBTs such as Takaishi et al. (2014) who presented the trade-off curve between turn-off loss and saturation collector voltage under extremely high current conduction conditions. In theory, the electro-thermal response of IGBTs critically depends on the collector tail current and collector-emitter saturation voltage.

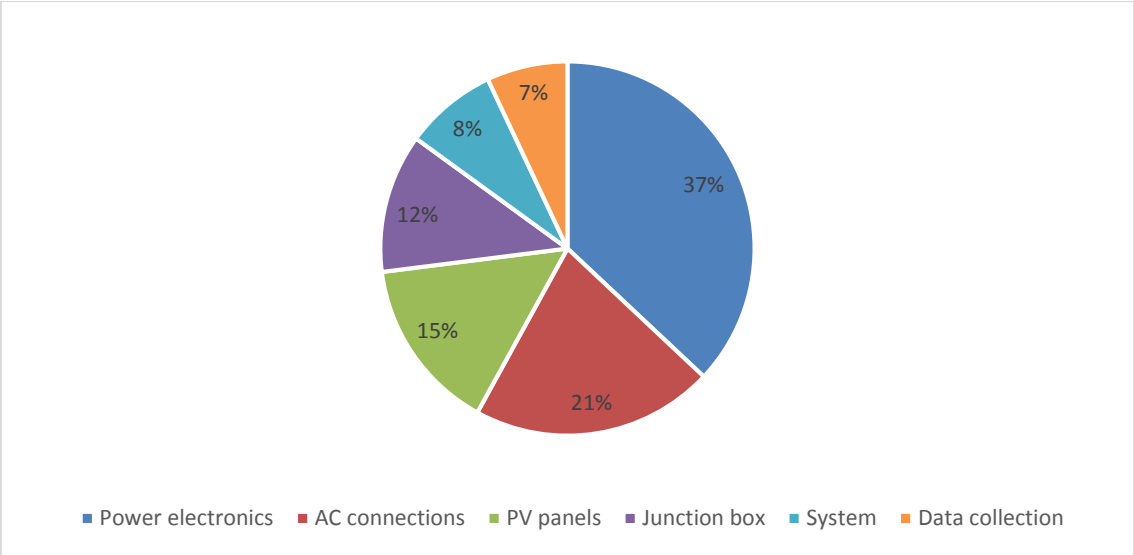

(a)

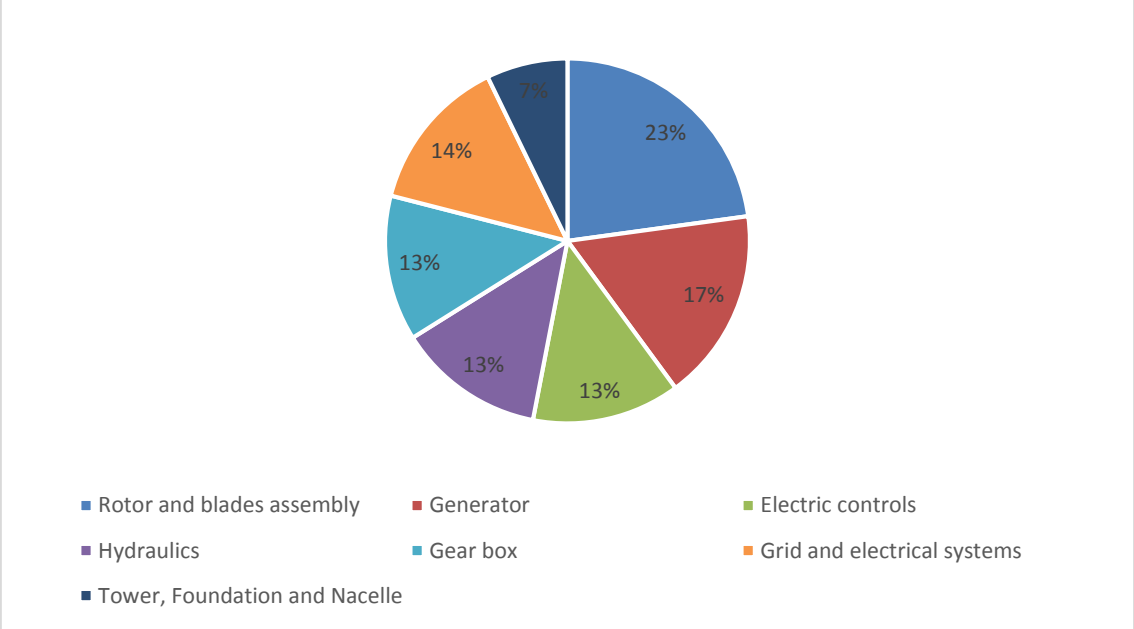

(b)

Figure 3. Failures causes in (a) PV systems, (b) wind turbines

Further support for this proposal was given by Tang et al. (2012), where the turn-off tail current at switching transient of an IGBT critically affected lifetime. Wu et al.(2012) have also proposed a Power System Computer Aided Design (PSCAD) compliant IGBT simulation model with the extension of temperature and on-time resistance dependent electro-thermal models. Batunlu et al. (2016) have integrated Simulink with dSPACE to establish real-time monitoring of the electro-thermal characteristics of IGBTs and achieved an accuracy of 97% in comparison to high-resolution thermal imaging. Recent advances in microcontrollers based measurement systems has led to the development of smart sensing technologies for a number of applications, which could be of great benefits

in monitoring thermal characteristics of IGBTs. Smart sensing units comprises sensing channels, signal conditioning unit, microprocessor for data analysis/decision making and data communication interface (wired or wireless). Kim et al.(2005) have reported by implementing wireless monitoring unit has significantly reduced the sensing development cost by approximate 95% .Smart sensors have been widely applied in structural health monitoring applications and for machinery monitoring purposes Becker et al (2009) and Yun et al. (2011). However, smart sensing technologies have not yet been fully utilised for monitoring of the electro thermal and lifetime condition of IGBTs.

This paper presents novel smart sensor architecture for autonomous monitoring of electro-thermal performance of IGBTs with capabilities of remaining lifetime predictions. Sensor's outputs were communicated to other systems such as SCADA and predictive maintenance systems. Section II in the paper reviews thermal characteristics of IGBTs. Section III presents design and structure of the proposed electro thermal monitoring and lifetime prediction system. Results and comments are given in Section IV. Conclusions and future work are depicted in the final section.

II. ELECTRO-THERMAL CHARACTERISTICS OF IGBT

a. Methodology

The IGBT drives collector-emitter current through switching signal from gate pin. To evaluate the electro-thermal stress, an equivalent schematic diagram of the proposed system is depicted in Figure 4 (a). FGA25N120ANTDTU IGBT by Fairchild is used in this paper. A hall-effect linear current sensor (ACS712 by Allegro) collected the collector current signals through IGBT. Whereas, an analogue temperature sensor, LM35DZ, is attached near to IGBT in order to measure its respective ambient temperature. IGBT emits electro-thermal heat under collector-emitter voltage until steady state temperature. Discussed by Batunlu et al. (2015) such thermal characteristics can be expressed with thermal resistances R_{th} and capacitances C_{th} as expressed by Equation (1).

$$T(s) = \sum_{k=1}^{N} \frac{1/C_{thn}}{s+1/(C_{thn}R_{thn})} P_L(s) \quad (1)$$

where T represents the emitted temperature and P_L is the power loss. The summation

annotation indicates equivalent thermal Foster network as shown in Figure 4 (b). Equation 1 represents the summation of nth order response system of RC circuits, which $R_{th,}.C_{th}$ is equivalent to the time constant of the system.

The IGBT was initially operated by a constant gate voltage and was heated until its temperature reached to steady state for thermal model parameter estimation. Temperature was monitored by thermal imaging and recorded in each 5 seconds. Based on the obtained transient temperature profile, thermal impedance for 3rd order Foster network has been interpolated using least square methods as derived by Batunlu et al. (2015) and it is shown in Table 1.

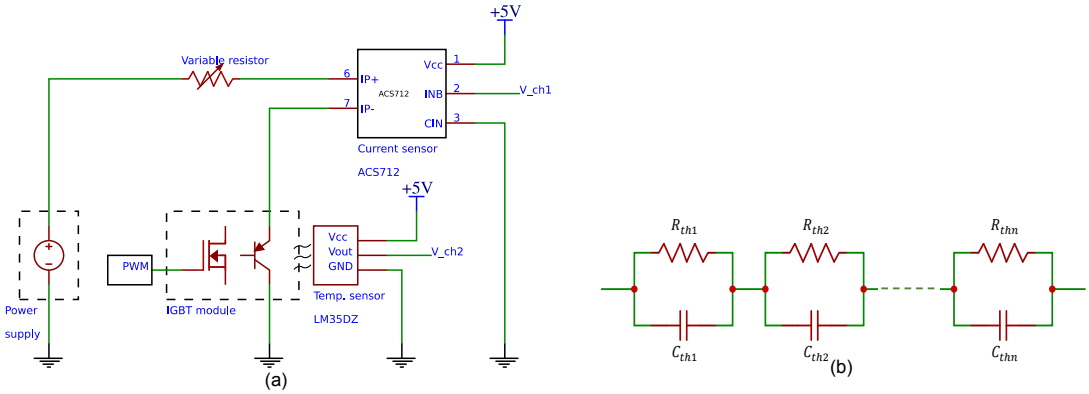

Figure 4. (a) Schematic diagram on measuring temperature and current of IGBT module (b) Foster Thermal Network

Table 1. Thermal Impedance Characteristics of IGBT

Device	Thermal Capacitance			Thermal Resistance		
	$C_{th,1}$	$C_{th,2}$	$C_{th,3}$	$R_{th,1}$	$R_{th,2}$	$R_{th,3}$
IGBT	0.134	0.294	26.89	0.343	0.329	0.322

Based on datasheet parameters, P_L was pre-requisitely calculated through simulations and experiments. A model equation of P_L is illustrated in Figure 5 (a). Surface map represents the interpolated data using two-dimensional surface fitting method, which is determined by Equation (2).

$$P_L(I_c,T) = -(2.283x10^{-3}) + (1.727x10^{-4})I_c + (5.577x10^{-3})T - (9.45x10^{-7})I_c^{\,2} + (3.076x10^{-5})I_cT - (3.503x10^{-3})^2T \quad (2)$$

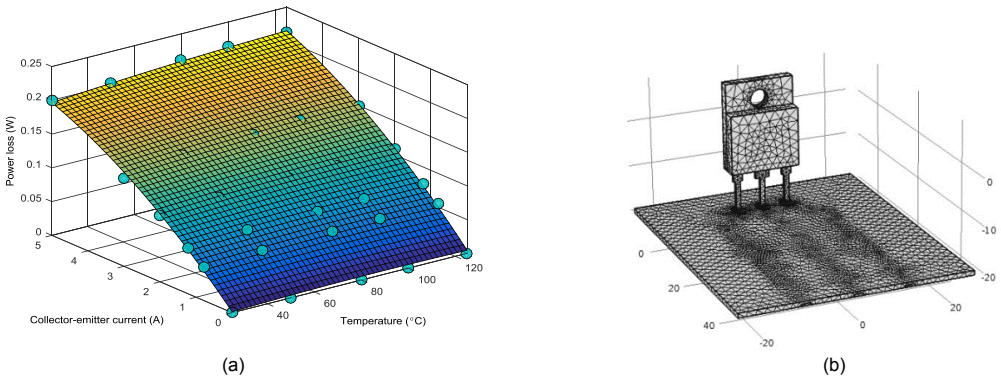

Figure 5. (a) Gradient map for PL estimation, (b) FE meshed model

b. Modelling and Simulation

COMSOL Multiphysics modelling software is used to simulate the electro-thermal model of IGBT. The 3D mesh model of IGBT is shown in Figure 5 (b). The heat distribution of the mesh model could be expressed in Equation (3):

$$\frac{\partial^2 T}{\partial x^2} + \frac{\partial^2 T}{\partial y^2} + \frac{\partial^2 T}{\partial z^2} + \frac{q}{k} = \frac{\rho.c}{k}\frac{\partial T}{\partial t} \tag{3}$$

where T is the temperature, k is the thermal conductivity, c is specific heat capacity, p is the mass density and q is the rate of generation of energy per unit volume. Simulation parameters are determined and discussed in previous paper by Batunlu et al. (2015).

III. PROGNOSIS ON OPERATIONAL LIFETIME BASED ON ELECTRO-THERMAL TEMPERATURE

a. Thermal Cycles Counting Algorithm

The cycle counting methodologies are as follows: Firstly, a temperature load history is collected; Cycle-counting algorithm is then performed to calculate number of thermal cycle across accumulation time; Finally the cumulative number of thermal cycles are summed and compared with referenced thermal cycle to failure to estimate operational life time as stated by Denk et al. (2015) and Downing and Socie (1982). To establish

prognosis on thermal fatigues of IGBT, two set of rainflow matrix, derived by Nieslony (2009) data are taken into account: referenced rainflow cycle function, $N_i(\sigma_a,\sigma_m)$ and rainflow cycle function of target monitoring device $n_i(\sigma_a,\sigma_m)$ where amplitude difference, σ_a, and mean, σ_m. A total life consumption could be formulated as shown in Equation (4).

$$L_c = \sum_{i=1}^{j} \frac{\mathrm{n_i}(\sigma_a.\sigma_m)}{\mathrm{N_i}(\sigma_a.\sigma_m)} \tag{4}$$

where i is the index of rainflow cycle function of the matrix, and j is the total number of rainflow cycle function of the matrix. The accumulated value of ratios n_i to N_i indicates the total life consumption coefficient L_c, which technically estimates that IGBT undergoes fatigue when L_c >1 and fails at L_c =1.

b. Proposed Autonomous extrema detection with online rainflow algorithm

Flowchart of autonomous extrema detection with rainflow algorithm is depicted in Figure 6.

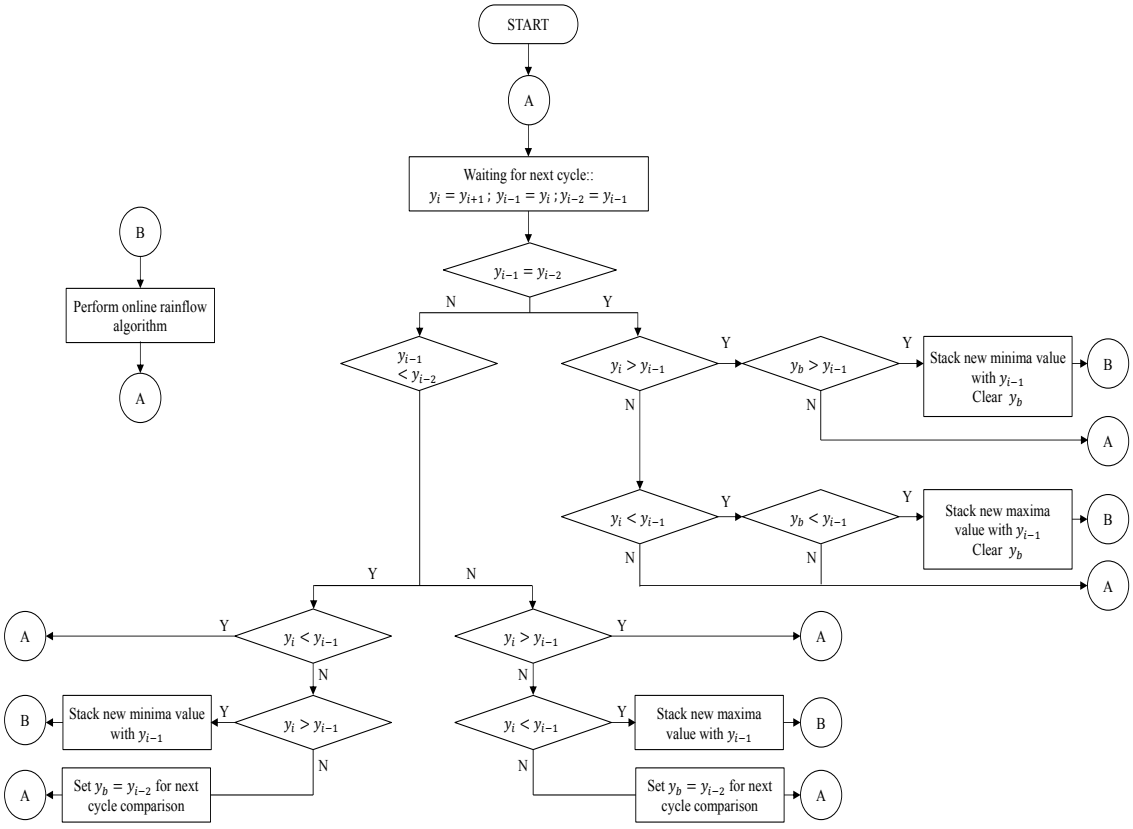

Figure 6. Equivalent flowchart of online extrema detection and rainflow algorithm

To perform detection algorithm, 3 sampling points at consecutive instances y_i (current

sample), y_{i-1} (sample from previous instance) and y_{i-2} (sample from previous two instances) are required. Firstly, y_{i-1} and y_{i-2} are compared, when $y_{i-1} > y_{i-2}$, it shows that y_{i-1} might be a potential maxima value and it is brought forward to compare with y_i. If $y_{i-1} > y_{i-2}$, this indicate that y_{i-1} is the maximum value between 3 points and a maxima at point *i-1* is noted. Subroutine is executed to perform online rainflow algorithm when extremas are detected. However, if $y_{i-1} = y_i$, its extrema detection is unknown and $y_{i-2}$is stored in a buffer, y_b for future comparison. Otherwise, y_{i-1} is not a maxima if $y_{i-1} > y_i$. During next cycle, new sampled data are loaded into the detection algorithm where the previous y values are shifted ($y_i = y_{i+1}, y_{i-1} = y_i, y_{i-1} = y_{i-2}$). If $y_{i-1} = y_{i-2}$, y_i is compared to check whether y_{i-1} is maxima or minima using y_b.

IV. SMART SENSOR DESIGN

Based on the monitoring framework in Figure (6), an equivalent monitoring strategy is established with a system-on-chip level 32-bit microcontroller unit. Table 2 shows the specification of two monitoring devices available in the lab.

Table 2. Technical specification of dSPACE module and microcontroller-based autonomous sensor

Specification	dSPACE monitoring panel (DS1006, DS2004ADC and DS5101PWMDAC)	32-bit microcontroller-based autonomous sensor
Price	Starting at £7000.00	Starting at £20.00
ADC resolution	16-bit	16-bit
Maximum sampling rate (2 channels)	1.25MHz	230kHz
Maximum input voltage range	±10V	0V to 3.6V
Power supply (individual module)	±5V, 2.0A	1.71V to 3.6V, operating current consumption down to 250 µA/MHz

dSPACE monitoring panel provides a mature platform to carry out real time monitoring as discussed by Batunlu and Albarbar (2015). The sampling rate of smart sensor is more than doubled switching frequency. Low power consumption of autonomous sensor also enables the potential power harvesting integration that is a trendy topic for remote wireless sensor network. To realise autonomous monitoring policy of IGBT electro-thermal monitoring, the autonomous sensor consists of three main modules, as shown in Figure (7). Autonomous sensor collects measurement signals from both sensing channels simultaneously using sample-and-hold module in the microcontroller unit. Analogue sensing channels of smart sensor are connected to ACS712 and LM35DZ. Digital signals are transmitted from sensing channels (ACS712) for current measurement) to processing

level for feature extraction and computation. Estimated electro-thermal characteristic of IGBT is then computed from measured signals, thus determining operational lifetime of the target device. Then, electro-thermal temperature difference is computed based on the new power loss value with internal thermal resistances. Thirdly, the calculated junction temperature is computed by adding up electro-thermal temperature difference with ambient temperature, measured using LM35DZ. This temperature data is loaded to perform extrema detection and online rainflow counting algorithm as previously discussed in section III. Total life consumption coefficient is updated and compared with threshold value. For remote communication, XBee 802.15.4 is used as wireless communication module for the developed system, which is connected through UART interface. The Baudrate is set to 230.4kBaud, enabling the writing speed of 43.41µs for an 8-bit character data from wireless communication module to site base station (Including parity bits). Two buffers are declared in microcontroller unit: power loss and electro-thermal models.

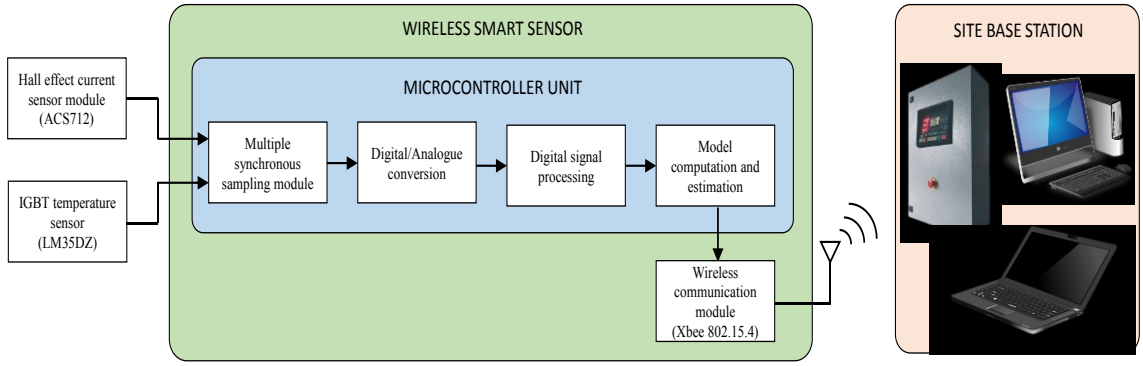

Figure 7. Smart sensor architecture for IGBT condition monitoring

V. SYSTEM'S PERFORMANCE AND ASSESSMENT

To validate the reliability of developed smart sensor system, thermal imaging is used as reference candidate due to its high accuracy and robustness in measuring temperature values. Lifetime estimation analysis was performed with dSPACE and a proposed smart sensor system for a sample temperature profile and performances of both systems was compared. Initially, IGBT circuit is connected to a power supply of 5V and maximum current supply of 3A. The initial switching frequency, f is set to 20kHz. The junction temperature response is shown in the Figure 8 (a). Then collector-emitter current rises when the resistance value of variable resistor bank, Rl is reduced, thus increases junction

temperature of the system. The temperatures relative to different current loads is shown in Figure 8 (b).

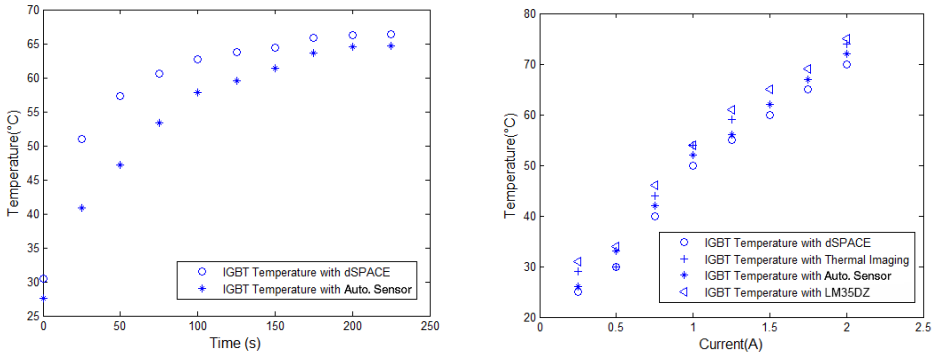

Figure 8. Temperature at (a) f=20kHz : R_l=1Ω; and (b) varied resistance

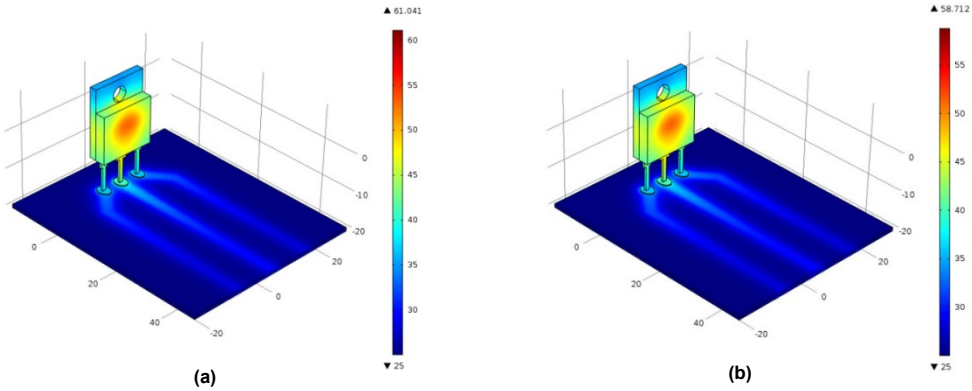

Figure 9. FE temperature profiles: (a) dSPACE; (b) smart sensor (f=20 kHz : R_l=1Ω)

The gradient map of both figures have similar heating distribution patterns, whereby at the centre of IGBT has reached the similarity of 94.22%. Both FEMs are then compared with thermal imaging as shown in Figure 9 & 10, showing the similarity of heat distribution behaviour (93.62% for dSPACE and 94.24% for smart sensor respectively).

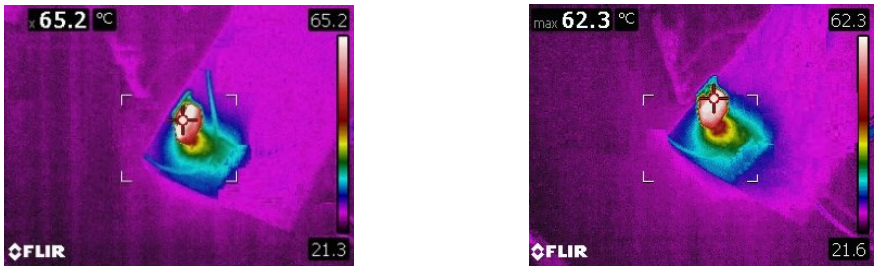

(a) (b)

Figure 10. Thermal imaging results: (a) dSPACE; (b) smart sensor (f=20kHz : R_l=1Ω)

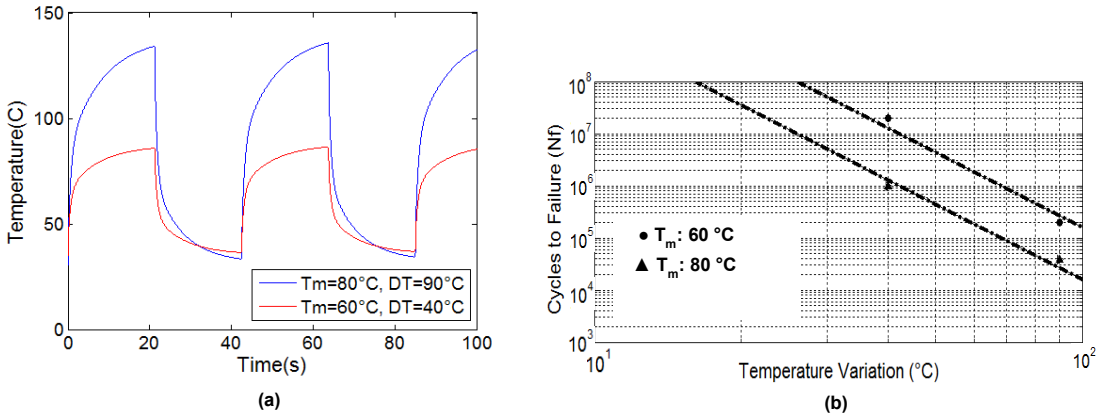

Figure 11. Accelerated power cycling test data temperature and lifetime curves

Lifetime analysis for the IGBT was performed for each system, individually. Number of cycles to failure was obtained by an accelerated power cycling test. Different test conditions were applied for the failure test. Temperature swing (ΔT) shown in Figure 11 (a) was adjusted as 90°C and 40°C with average temperatures (T_m) of 80°C and 60°C, respectively.

In both systems, several devices were run until they fail. Then temperature profiles were used to define Coffin-Manson-Arrhenius model, stated by Blaabjerg et al. (2012) to calculate cycle failure data as a function of mean temperature, T_m and variation, ΔT as expressed in Equation (5).

$$N_f = A(\Delta T_j)^{\alpha} . e^{\left(\frac{E_a}{k_b . T_m}\right)} \tag{5}$$

where N_f is expected number of cycles to failure, k_b is Boltzman constant, 1.38x10^{-23} J·K−1, E_a is the activation energy, 1.3 x 10^{-19} J, A and α are the constants, 610 and -5, respectively which are fitted by least square method. The lifetime curves are presented as shown in Figure 11 (b). An example profile was generated by varying the resistive load and the resultant temperature profiles with both systems can be seen in Figure 12 (a) & (b), respectively.

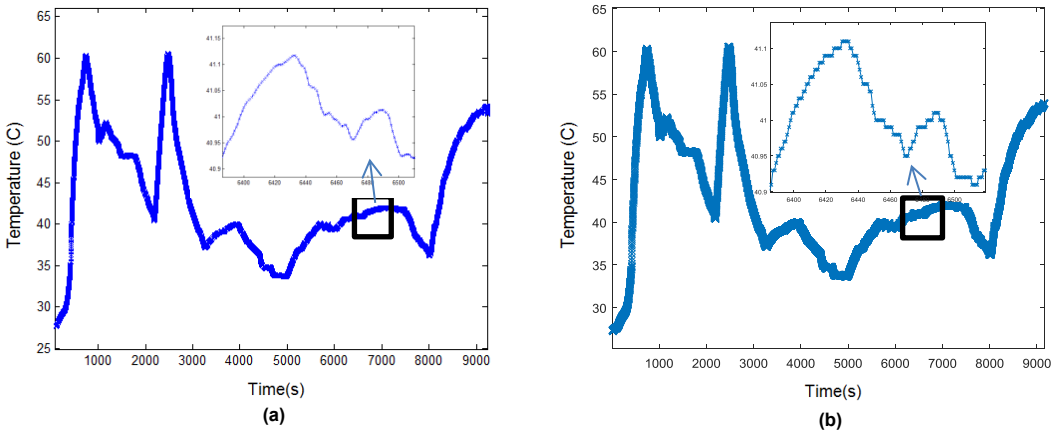

Figure 12. Temperature profiles: (a) dSPACE & (b) smart sensor

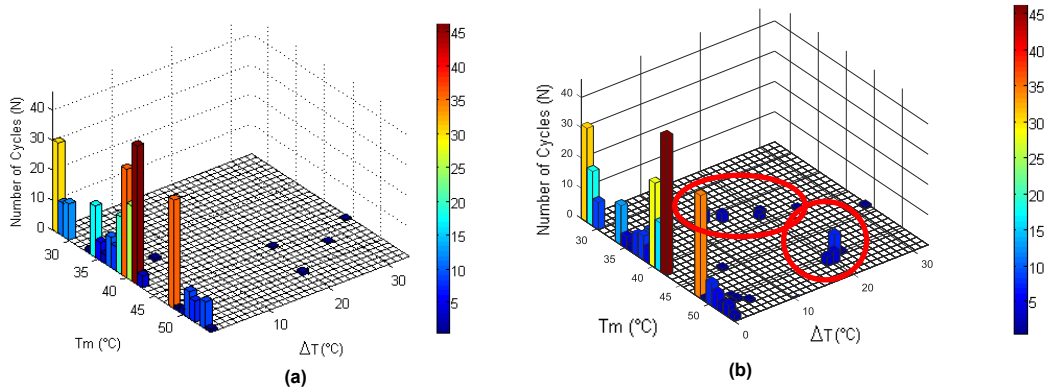

Figure 13. Number of cycles found with (a) dSPACE and (b) Smart Sensor

Based on the sample temperature the calculated numbers of cycles in both systems are presented in Figure 13 (a) & (b), respectively. The smart sensor was able to detect higher cycles especially at higher ΔT values. The offline Rainflow algorithm method applied through the dSPACE performance is quite similar to with smart sensor at lower temperature swing values. This is due to the higher capability of sample detection with a higher sampling rate time. However, higher sample data caused the offline Rainflow algorithm method to confuse at higher temperature picks which results in inaccuracies on cycle detection. For instance, the difference is visible when the ΔT=20°C at 50°C of mean temperature. The offline method was able to detect only 4 cycles at whereas the actual cycle is 11, which was observed by the proposed online method. There are also considerable cycles for lifetime consumption (LC) around 35 °C of mean temperature at various ΔT levels from 10-20 °C. The LC for both systems can be depicted in Figure 14 (a) & (b).

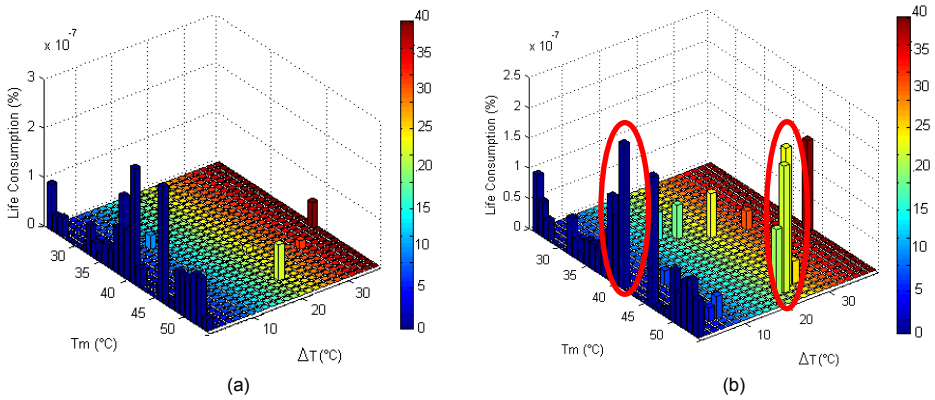

Figure 14. Lifetime Consumption with (a) dSPACE and (b) Smart Sensor

Similar total LC was observed with both systems at lower temperature swing levels but the proposed smart sensor based system was able to detect more LC as a result of higher peak detection, expectedly. The total LC is 18.2 x 10^{-7} with the dSPACE system based offline method and it was 24.8 x 10^{-7} with the online method. Thus, approximately 1.4 times higher LC was observed with smart sensor system under same loading and environmental conditions compared to the dSPACE system based offline method. As it can be observed at highlighted precision on Figure 14 (b), less amount of number of cycle (i.e. 4) at temperature variation of 35 °C at 41 °C mean temperature caused approximately same amount of life consumption with higher number of cycles (i.e. 42) at low temperature variation of 1°C.

VI. CONCLUSION

An inexpensive and accurate microcontroller-based autonomous sensor, for monitoring electro thermal characteristics of IGBT, was designed and implemented in this work. The developed system calculates the IGBT's thermal behaviour through non-intrusive measurement of its currents and embedded computation models. The performance of developed sensor was experimentally verified and found to achieved 95% average accuracy compared to, professional and matured technology of, a thermal imaging camera. Operational lifetime result has also been successfully estimated using predefined analytical model and rainflow extraction method. Due to the limitation of the microcontroller's analogue to digital conversion, the developed sensor could not capture power disturbances of the IGBT at toggling stage. However, results showed that does not really have any effect ultimate estimation of IGBT's junction temperature. The calculated number of cycles and life consumption are accurate enough. In conclusion, the developed

smart sensor is expected to pave the path for full adoption as a potential monitoring tool for power electronic convertors and other semiconductor devices.

REFERENCES

Arabian-Hoseynabadi H., Oraee H., Tavner P., (2010) ‘’Failure Modes and Effects Analysis (FMEA) for wind turbines’’ Electrical Power and Energy Systems 32 (2010) 817–824.

Batunlu C. and Albarbar A., (2015) “A Technique for Mitigating Thermal Stress and Extending Life Cycle of Power Electronic Converters Used for Wind Turbines,” Electronics, vol. 4, no. 4, pp. 947–968, Nov. 2015.

Batunlu C. and Albarbar A., (2016) “Real-time system for monitoring the electro-thermal behaviour of power electronic devices used in boost converters,” Microelectronics Reliability. vol. 62, pp. 82–90, July 2016.

Batunlu C. and Albarbar A., (2015) “Towards More Reliable Renewable Power Systems - Thermal Performance Evaluation of DC/DC Boost Converters Switching Devices,” International Journal of Power Electronics and Drive Systems (IJPEDS), vol. 6, no. 4, pp. 876–887, Dec. 2015.

Becker T., Kluge M., Schalk J., Tiplady K., Paget C., Hilleringmann U., and Otterpohl T., (2009) “Autonomous Sensor Nodes for Aircraft Structural Health Monitoring,” Sensors Journal, IEEE, vol. 9, no. 11, pp. 1589–1595, Nov. 2009.

Blaabjerg F., Ma K., and Zhou D., (2012) “Power electronics and reliability in renewable energy systems,” in2012 IEEEInternational Symposium on Industrial Electronics (ISIE), 2012, pp. 19–30.

Denk M., Bakran M.-M., Denk M., and Bakran M.-M., (2015) “Online Junction Temperature Cycle Recording of an IGBT Power Module in a Hybrid Car, Online Junction Temperature Cycle Recording of an IGBT Power Module in a Hybrid Car,” Advances in Power Electronics, Advances in Power Electronics, vol. 2015, 2015, p. e652389, Mar. 2015.

Downing S. D. and Socie D. F., (1982) "Simple rainflow counting algorithms," International Journal of Fatigue, vol. 4, no. 1, pp. 31–40, Jan. 1982.

Kim Y.-J., Lee K.-C., Hwang D.-H., and Kang D.-S.,(2005) "Technologies and cost evaluation of condition monitoring and diagnosis system under ubiquitous environment," in Proceedings of 2005 International Symposium on Electrical Insulating Materials, 2005. (ISEIM 2005), 2005, vol. 3, p. 857–860 Vol. 3.

Natsheh E, Natsheh A, Albarbar A, (2013), Intelligent Controller for Managing Power Flow within Standalone Hybrid Power Systems. IET Science, Measurement & Technology, 7(4), 191-200.

Natsheh E, Albarbar A, (2012). Solar Power Plant Performance Evaluation: Simulation and Experimental Validation. J. Phys.: Conf. Ser. 364 012122 doi:10.1088/1742-6596/364/1/012122.

Natsheh E, Albarbar A (2014), An Automated Tool for Solar Power Systems, Applied Solar Energy, 50, (4), 221-227.

Niesłony A., (2009)"Determination of fragments of multiaxial service loading strongly influencing the fatigue of machine components," Mechanical Systems and Signal Processing, vol. 23, no. 8, pp. 2712–2721, Nov. 2009.

Takaishi J., Harada S., Tsukuda M., and Omura I., (2014)"Structure oriented compact model for advanced trench IGBTs without fitting parameters for extreme condition: Part II," Microelectronics Reliability, vol. 54, no. 9–10, pp. 1891–1896, Sep. 2014.

Tang Y., Wang B., Chen M., and Liu B., (2012)"Simulation model and parameter extraction of Field-Stop (FS) IGBT," Microelectronics Reliability, vol. 52, no. 12, pp. 2920–2931, Dec 2012.

Wu R., Wen J. L., Han J., Chen Z., Wei Q., Jia N., and Wang C.,(2012) "A Power Loss Calculation Method of IGBT Three-Phase SPWM Converter," in 2012 Second International Conference on Intelligent System Design and Engineering Application (ISDEA), 2012, pp. 1180–1183.

Yun G. J., Lee S.-G., Carletta J., and Nagayama T., (2011)"Decentralized damage identification using wavelet signal analysis embedded on wireless smart sensors," Engineering Structures, vol. 33, no. 7, pp. 2162–2172, Jul. 2011.